Flow Visualization in Mechanical Heart Valves: Occluder Rebound and Cavitation Potential

V. Kini,[1] C. Bachmann,[1] A. Fontaine,[2] S. Deutsch,[2] and J. M. Tarbell[3]

Artificial Heart Laboratory, [1]The Bioengineering Program, [2]The Applied Research Laboratory, [3]The Bioengineering Program and Department of Chemical Engineering, The Pennsylvania State University, 115 Hallowell Building, University Park, PA

Abstract—High density particle image velocimetry, with spatial resolution of $O(1 \text{ mm})$, was used to measure the effect of occluder rebound on the flow field near a Bjork–Shiley Monostrut tilting-disk mitral valve. The ability to measure two velocity components over an entire plane simultaneously provides a very different insight into the flow compared to the more traditional point to point techniques (like Laser Doppler Velocimetry) that were utilized in previous investigations of the regurgitant flow. A picture of the effects of occluder rebound on the fluid flow in the atrial chamber is presented. Specifically, fluid velocities in excess of 1.5 m/s traveling *away* from the atrial side were detected 3 mm away from the valve seat in the local low pressure region created by the occluder rebound on the major orifice side where cavitation has been observed. This analysis is the first spatially detailed flow description of the effects of occluder rebound on the flow field past a tilting-disk mechanical heart valve and further reinforces the hypothesis that the rebound effect plays a significant role in the formation of cavitation, which has been implicated in the hemolysis and wear associated with tilting-disk valves *in vivo*. © *2000 Biomedical Engineering Society.*
[S0090-6964(00)00704-9]

Keywords—Particle image velocimetry, Heart valve, Cavitation, Regurgitation.

INTRODUCTION

Cavitation is the formation of vaporous (or gaseous) cavities (bubbles) in low pressure regions of a flow field and their subsequent collapse during pressure recovery. Vaporous cavity formation and collapse on mechanical heart valves occur within a few milliseconds after valve closure and have been observed on the upstream side of various valve types *in vitro* using stroboscopic videography on our group.[19] Vaporous cavitation can damage valve materials, and there is evidence of surface pitting on valves explanted from animals and humans which indicates that cavitation does indeed occur *in vivo*.[7] Using a high fidelity pressure transducer mounted on the inlet cannula of a Penn State electric ventricular assist device (VAD) implanted in a calf, we have recently observed direct evidence of vaporous cavitation *in vivo* in the form of a pulse of high frequency (several hundred kilohertz) pressure fluctuations appearing a few milliseconds after valve closure.[18] In earlier *in vitro* studies we correlated such pressure fluctuations with the visual observation of vaporous cavitation bubbles.[6,8] In addition to damaging valve materials, vaporous cavitation, or concomitant fluid stresses associated with valve closure, can also damage blood. This was demonstrated *in vitro* by measuring the rate of plasma-free hemoglobin (PFHG) release under operating conditions known to produce vaporous cavitation and observing a marked increase in the hemolysis rate.[6] Recent studies in calves with a Penn State electric VAD, have shown an increase in PFHG release and lactate dehydrogenase release under elevated vaporous cavitation conditions.[16,17]

The mechanisms of cavitation on heart valves are not well understood at the present time. There does, however, seem to be agreement that elevated valve closing velocity and deceleration, which are related to elevated dP/dt, play a role in cavitation because they lead to a reduction in local pressure through a ''water hammer'' mechanism.[3,13,14,17] Other mechanisms, which are thought to contribute to local pressure reduction, are squeeze flow, tension waves, valve rebound, and vortex formation.

On the Medtronic–Hall valve, the major site of vaporous cavitation bubble formation is around the valve stop on the major orifice side of the disk.[9,10,19] It has been suggested that this location is favored because at the instant of impact between the high velocity occluder tip and the stop, the fluid is ''squeezed'' between the stop and the occluder, and a local flow field with high velocity (and implicitly, low pressure) is created which favors cavitation.[9,10] Vaporous cavitation is also observed on the minor orifice side of the Bjork–Shiley Monostrut (BSM) valve in the region where the occluder impacts the stop.[19] It is possible that squeeze flow contributes to cavitation at this location and calculations

Address correspondence to J. M. Tarbell; electronic mail: jmt@psu.edu
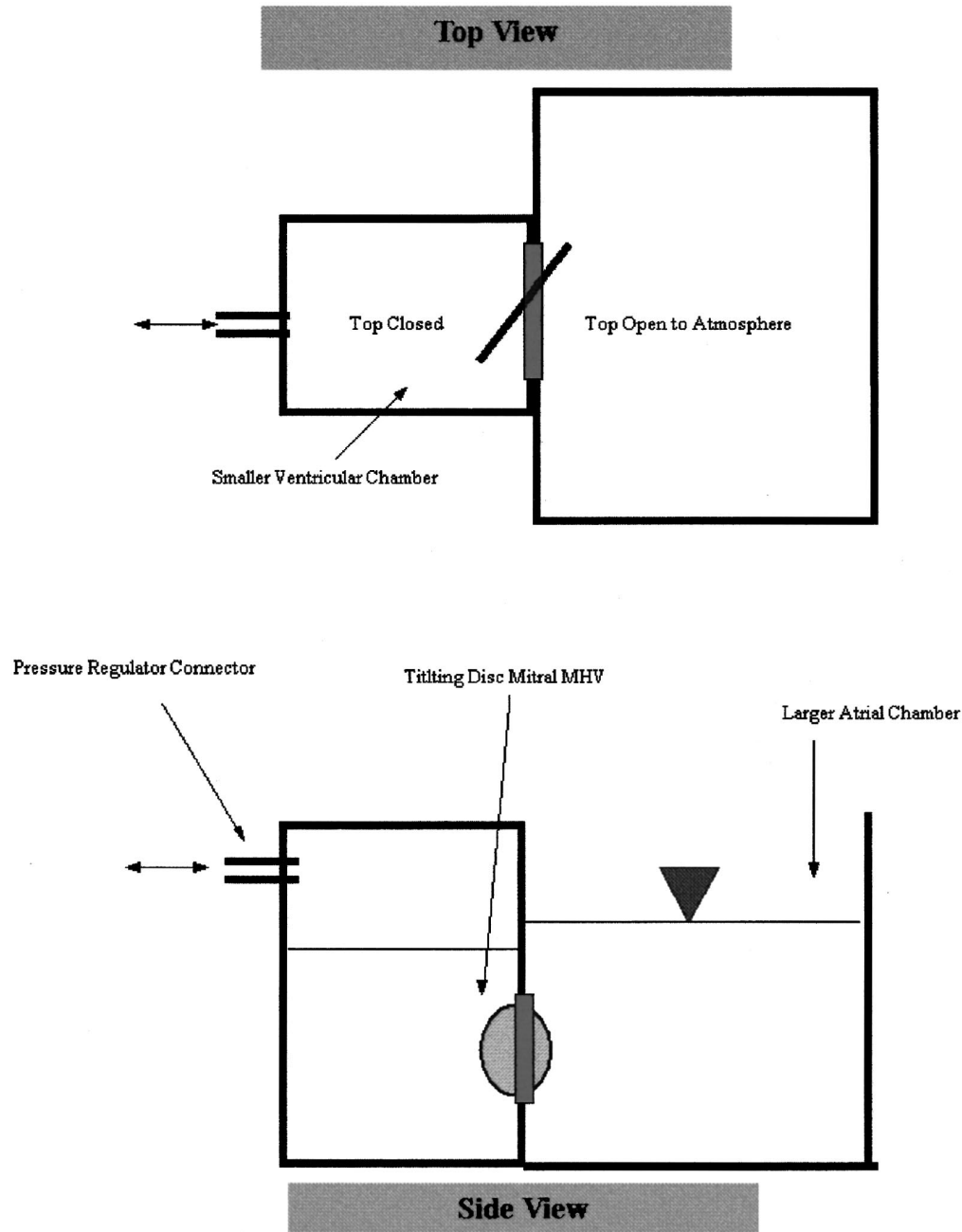
FIGURE 1. Schematic view of the MHV chamber used for PIV studies. The diagram shows a tilting-disk mitral valve in the valve holder. The larger atrial chamber is held open to the atmosphere. The smaller ventricular chamber is closed and connected to a pneumatic pressure regulator. The regulator provides the systolic ejection pressure that shuts the mitral valve. The valve is then allowed to open until the fluid levels equalize. There is no true forward flow. This represents a type of one-shot valve closure chamber setup.

have been made[2,11] which showed fluid jet velocities in the squeeze flow that far exceeded the occluder tip velocity. On the other hand, the major site for vaporous cavitation on the BSM valve is around the edge of the occluder on the major orifice side of the valve.[6] There is no closing stop on this side of the valve, and thus it is less likely that squeeze flow is a dominant mechanism

for cavitation in this region. One possible mechanism is what has been referred to in the literature as ''vortex cavitation.''[15] Vortex cavitation is initiated at the low pressure center of a vortex. For valve flows such a vortex might be formed in two ways. First, the closing valve is moving relative to the surrounding fluid which produces lift on the valve. This lift is relieved at closure
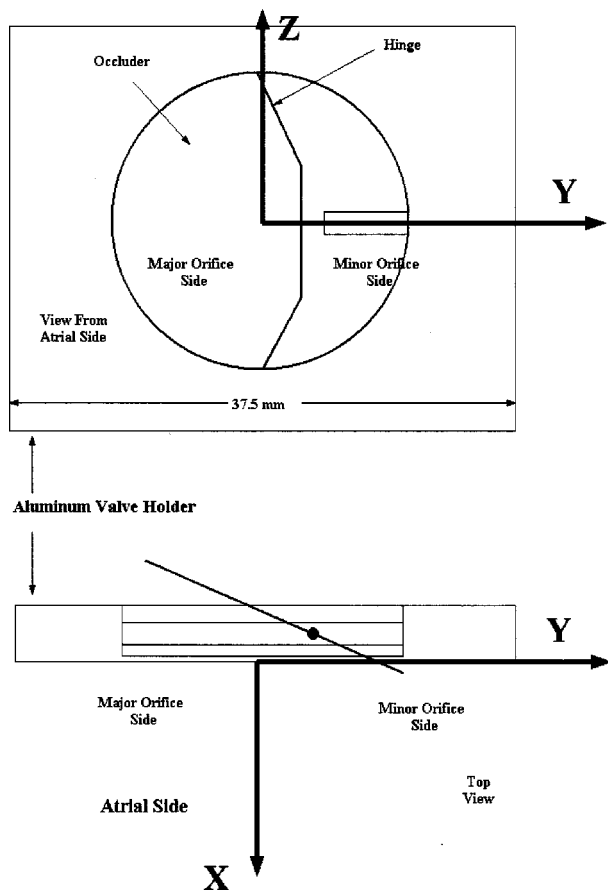
FIGURE 2. Axes definitions. The diagram shows a tilting-disk BSM valve in the valve holder. The central plane of the valve was defined as $z=0$. The x axis was measured from the valve holder and into the atrium. Due to the valve holder recess and proximity of the wall, our first point is approximately 3 mm from the valve seat on the atrial side. The y axis was measured from the center of the valve.

through the formation of a stopping vortex (analogous to a starting vortex for an aircraft wing). The relative velocity would vary with valve geometry and material, so that the corresponding vortex generated would have different strengths. Second, the motion of the valve across the narrow gap near closure will tend to roll the gap fluid up into what has been termed a ''scraping vortex'' in turbomachinery research.[5] In the case of the Bjork–Shiley monostrut, for example, one might expect the vortex produced on the major orifice side of the valve would be most intense since the occluder tip velocity is highest there. Again, this scraping vortex will be a function of valve geometry. These hypothesized scraping vortices have not yet been observed directly in experiments. Another possible mechanism for the formation of vaporous cavitation is the tension wave (or local pressure drop) caused by the sudden stopping and rebound motion of the occluder. The magnitude of this pressure drop is related to the speed of the rebounding occluder and is

maximum along the tip of the major orifice side. Indeed, it is in this region that the majority of cavitation field observations have been made,[8] therefore it appears that this local pressure drop below the atrial pressure is one of the contributing factors to the formation of the cavitation field. In this particle image velocimetry (PIV) based investigation the effect of valve rebound on the local fluid flow patterns and thereby, by inference, on the local pressures and the cavitation potential is presented.

Most of today's mechanical heart valve (MHV)-related fluid dynamics measurements are made with point-based techniques like laser-Doppler velocimetry. Such techniques do not convey the sense of spatial disturbances in the flow field as is commonly found in MHV applications. PIV, on the other hand, being an instantaneous, two-dimensional (2D) plane-based approach, is capable of providing new insight into the complex transient fluid dynamics of MHVs.

The PIV approach, unlike point-based techniques, provides quantitative whole-field fluid velocity information and thus contributes to a new perspective on flow phenomena. Specifically, the PIV measurement process involves the following: seed particles are suspended in the fluid to follow the flow of the fluid and provide a signal. When a light sheet illuminates a thin slice of the flow field, the illuminated seed particles scatter the light and a camera placed at right angles to the light sheet detects these particles. The light sheet is pulsed (switched on and off very quickly) twice at a known interval (t). The first pulse of the laser freezes images of the initial positions of seed particles onto the first frame of the camera. The camera frame is advanced and the second frame of the camera is exposed to the light scattered by the particles from the second pulse of laser light. There are thus two camera images, the first showing the initial positions of the seeding particles and the second showing their final positions due to the movement of the flow field. The two camera frames are then processed to find the velocity vector map of the flow field. This involves dividing the camera frames into small areas called interrogation regions. In each interrogation region, the displacement (s) of groups of particles between frame 1 and frame 2 is measured using correlation techniques (which are implemented using fast Fourier tranform algorithms).[1] The velocity vector of this area in the flow field is then calculated using the equation

$$V = k(s/t)$$

where k is the object:image scale factor between the camera's charge coupled device (CCD) chip and the measurement area (i.e., conversion of displacements in pixels to displacements in physical length). This is re-

peated for each interrogation region to build up the complete 2D-velocity vector map. A more detailed account of the PIV approach may be found in the article by Adrian.[1]

METHODS

In this study the ''one-shot'' experimental setup was very similar to the one described by Chandran and Aluri.[4] As shown in Fig. 1, the two-chambered valve box was manufactured from acrylic for optical access. The laser side of the chamber was fitted with optical-grade glass windows to prevent laser-induced damage to the acrylic. The smaller ventricular chamber was sealed and connected to the pneumatic pressure regulator system. The larger atrial chamber was held open to atmosphere. An anodized aluminum valve holder was placed between the chambers and securely held the prosthetic mitral valve (BSM, 27 mm, carbon occluder, with a rubber ring) under study. The axes, as used in this analysis, are shown in Fig. 2. The central plane of the valve was defined as $z = 0$. The x axis was measured from the edge of the valve holder and into the atrium. Allowing some distance from the wall to eliminate the slight laser glare, we were able to estimate the flow field on the atrial side as close as ~3 mm from the actual seat. The y axis was measured from the center of the valve, as seen in Fig. 2. The atrial pressure head measured at the valve center was kept almost constant at a mean of 5–7 mm Hg. The total systolic duration (shut the valve and keep it closed) was held constant at 300 ms. At the end of this time, the pressure was released such that the fluids in both chambers leveled out again. Note that in this study there is no true suction for ventricular filling. The forward flow volume is exactly equal to the back flow volume. In the case of true pulsatile flow, the forward flow volume is an order of magnitude larger. Only events as observed in this type of one-shot valve closure process were investigated. The pressure in the ventricular chamber was measured at valve centerline, ~30 mm away from the valve seat, using a Millar microtip pressure transducer inserted into the sealed ventricle. The peak ventricular pressure was set at a physiologically realistic ~120 mm Hg and the dp/dt of closure calculated over the whole closure period exactly along the lines of Chandran *et al.*[4] was set at ~1200 mm Hg/s. The *instantaneous* value of dp/dt measured 20 ms before the impact of the occluder was ~2200 mm Hg/s. The typical pressure trace appears in Fig. 3. Note that under these operating conditions, no cavitation was observed. The operation was deliberately kept in the subcritical range because the presence of the cavitation field impedes flow visualization experiments. The study was focused on determining fluid flow trends that explain, by inference, the presence, structure, and nature of cavitation fields when observed in the critical range.

The blood analog fluid used was a solution of 60% water, 40% glycerol mixture with viscosity of 3.5 cP, and a density of 1.1 g/cm^3 at room temperature. The fluid was seeded with silver-coated 10 μm hollow glass spheres (Potters Industries, Parsippany, NJ) to allow for PIV imaging.

As a preliminary study, the valve closure and occluder rebound events were visually inspected using a high speed CCD camera (Kodak MotionCorder SR 10000) and the exact instants of occluder-seat contact were determined using a high frequency response accelerometer.

In the PIV setup two pulsed Nd–yttrium–aluminum–garnet (YAG) (Surelite II, Continuum Inc, Santa Clara, CA) lasers were used to illuminate the images. The laser generates output in the infrared at 1064 nm and this beam is then passed through a frequency doubler that is capable of outputting light in the green at 532 nm. The lasers individually could not be operated beyond 10 Hz, but timing the pair allowed the PIV images to be separated by as little as 50 μs. Thus, the laser-pulse separation was four orders of magnitude larger than the width of each individual pulse (9 ns). The lasers were capable of delivering a maximum of 250 mJ per pulse, but for our study ~80 mJ proved sufficient for illumination. A beam-combination optics and cylindrical lens system was used to convert the two pulsed beams into pulsed sheets. The average thickness of the laser sheet as it passes the atrial region of the mitral valve chamber was kept at about 1 mm.

The PIV images were acquired in an online format using a PIVCAM (TSI Inc, St. Paul, MN, Model 630046) CCD camera with a resolution of 1024×1018 pixels and maximum speed of 30 frames/s. A Nikon AF Micro-Nikkor 60 mm zoom lens was used to decrease the field of view. The images were divided into staggered zones of interest of about 1 mm×1 mm and the PIV analysis was subsequently performed using the Insight PIV Software (TSI, St. Paul, MN). The flow maps as presented represent an ensemble average of 30 instantaneous flow maps taken at a given phase of the valve motion cycle. The analysis when performed on a 300 MHz Pentium II Micron PC operating on the Windows-NT Workstation platform could output about 50 vectors per second on the average.

Two markers on the valve holder, separated by 1.5 in., were used for physical scaling of the image. It was observed that while using the point and click approach to estimating the number of pixels in the 1.5 in. length, there was an uncertainty of approximately 3 pixels in an average total of 760 pixels. We can then estimate the uncertainty in length scale as
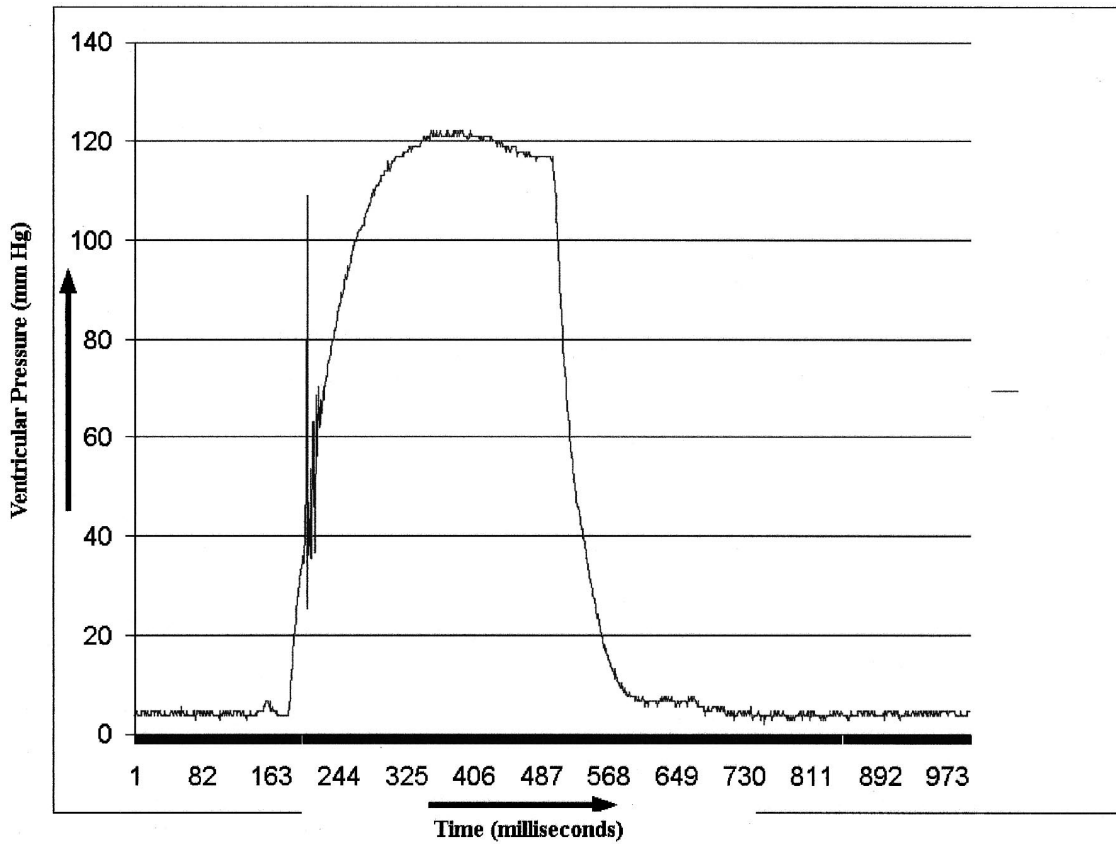
FIGURE 3. Trace of the ventricular pressure as measured ~30 mm from the valve. The peak ventricular pressure was set at 120 mm Hg and the characteristic average dp/dt of closure (calculated exactly along the line of Chandran *et al.*[4]) was adjusted to ~1200 mm Hg/s. The sharp pressure spike indicates the valve closure event. Note that there is no true forward flow, and this is a type of one-shot valve operation.
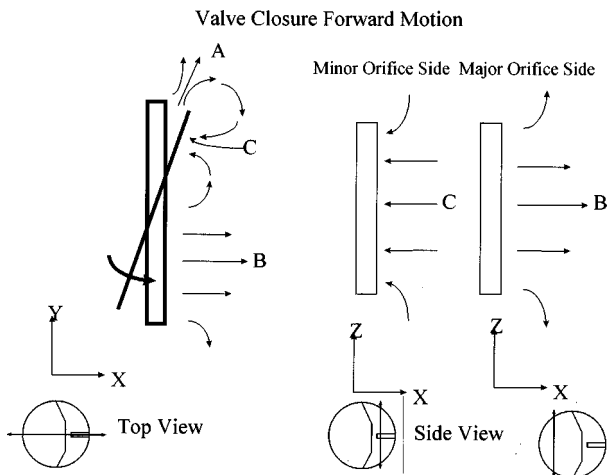

FIGURE 4. A schematic depicting the flow patterns during valve closure forward motion, as seen in the central plane (z=0), the vertical plane (y=+6 mm) on the minor orifice side and the vertical plane (y=−6 mm) on the major orifice side. Note that the actual flow map begins ~3 mm away from the actual valve seat.
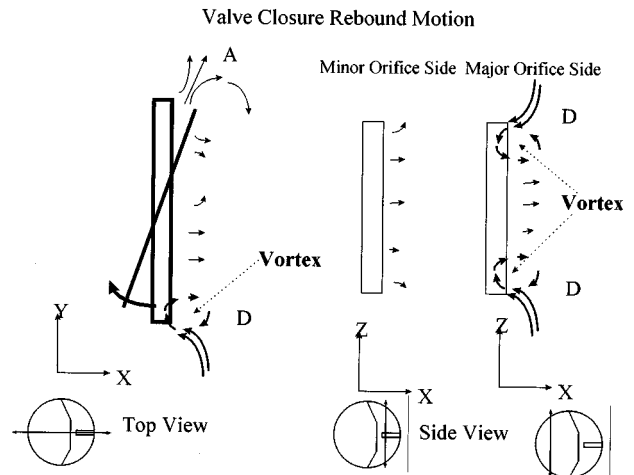
FIGURE 5. A schematic depicting the flow patterns during valve closure rebound motion, as seen in the central plane (z=0), the vertical plane (y=+6 mm) on the minor orifice side and the vertical plane (y=−6 mm) on the major orifice side. Note that the actual flow map begins ~3 mm away from the actual valve seat.

$$U_x = \frac{760 \pm 3}{1.5(2.54)\,10} = 19.9475 \pm 0.0787 \;\; \text{pixels/mm},$$

$$\text{or, } 50.1316 \pm 0.1970 \;\; \mu\text{m/pixel}.$$

The uncertainty in fixed pulse separation of 100 μs in any given instantaneous map was to the order of 0.1 μs. This leads to a derived uncertainty in the velocity scale in any given instantaneous flow map that may be estimated as

$$U_x = \left(\frac{\dfrac{n(50.1316 + 0.1970)\,10^{-6}}{(100 - 0.1)\,10^{-6}}}{\dfrac{n\,50.1316 \times 10^{-6}}{100 \times 10^{-6}}} - 1 \right) 100$$

$$= \left(\frac{0.5038}{0.5013} - 1 \right) 100 \approx 0.5\%.$$

Note that in the ensemble averaging process there is a phase uncertainty (a time bin width) of 0.5 ms. However, this uncertainty associated with the velocity as depicted in an averaged flow map is difficult to estimate.

The PIV setup was initially validated using a 5 mm exit-diameter nozzle with a 3 ft water head emptying into the large atrial chamber. Actual flow rate measurements were used to confirm the average velocity at nozzle exit as predicted by the PIV study.

RESULTS AND DISCUSSION

The local ventricular pressure trace around the event of valve closure was examined. The rebound effect could be observed on high-speed video and was confirmed using an accelerometer. The first pressure spike indicates the first instant of valve closure. The occluder then rebounds, draws back, and goes through another forward closure motion before it strikes the seat a second time approximately 10 ms later. The valve then rebounds again, albeit with reduced amplitude, and closes again ~10 ms later. A third rebound was barely visible using the pressure and accelerometer curves.

A schematic representation of the regurgitant flow patterns typically associated with valve closure forward motion and rebound in tilting-disk valves is provided as an aid to visualization in Figs. 4 and 5, respectively. In the central horizontal plane ($z = 0$ mm) there are two distinct flow regions: a minor orifice and a major orifice region. During the occluder's forward closure motion, as depicted in Fig. 4, the flow on the atrial side shows a striking minor orifice jet directed at an angle (marked A). Here the fluid is driven from the ventricle to the atrium by the global pressure gradient, against the *local* direction of motion of the occluder. On the major orifice side,

the fluid (associated with the closure volume) is traveling *in* the local direction of motion of the occluder and indicates a smoother parabola-like profile (marked B). In the transition between the minor and major orifice zones, a vortex (~8 mm) is formed which is caused by the fluid on the atrial side of the minor orifice following the direction of motion (*against* the *global* pressure gradient) of the occluder's minor side (marked C). This pattern appears to be typical of valve closure forward motion.

During the occluder's rebound motion, as depicted in Fig. 5, the flow on the atrial side shows the same minor orifice pressure-driven jet (marked A) directed at an angle, now traveling along with the *local* direction of motion of the occluder. On the major orifice side, however, the sudden stoppage and subsequent rebound causes the local pressure to drop below the atrial reservoir pressure. This pressure drop retards the fluid on the atrial side and appears to draw fluid in along the periphery (where the inertia of the fluid during forward closure motion was small) leading to flow reversal and an extremely tight vortex (marked D). This short lived three-dimensional (3D) vortex is so small that it is below the resolution range $[O(1\,\text{mm})]$ of our PIV setup, and though its presence was detected in the flow map and confirmed using high speed video, it is impossible to come up with a realistic estimate of its strength at this time.

The experimental results for the flow patterns in the central plane ($z = 0$ mm) during forward closure motion of the occluder with typical regions A, B, and C, is shown in Fig. 6. The experimentally determined flow patterns associated with region C, in the $y = 6$ mm vertical plane on the minor orifice side during valve closure forward motion is depicted in Fig. 7. The flow in this plane is following the motion of the minor orifice side of the occluder. Note the central depression of the velocity profile. This is probably caused by the fact that the occluder is not a flat disk, but rather has a curvature such that the actual distance to the occluder is at a maximum in the central region. On the other hand, the experimentally determined flow patterns associated with region B, in the $y = -6$ mm vertical plane on the major orifice side during valve closure forward motion are depicted in Fig. 8. It can be seen that in this plane, measured at least 3 mm away from the valve seat, there is a recirculation zone as the fluid enters the sudden expansion zone in the atrial chamber.

Contrasting the earlier with the patterns during occluder rebound, the flow patterns in the central plane ($z = 0$ mm) during rebound motion of the occluder with typical regions A and D, are shown in Fig. 9. The experimentally determined flow patterns in the $y = 6$ mm vertical plane on the minor orifice side during valve closure forward motion are depicted in Fig. 10. Here it can be seen that ~3 mm away from the valve seat the
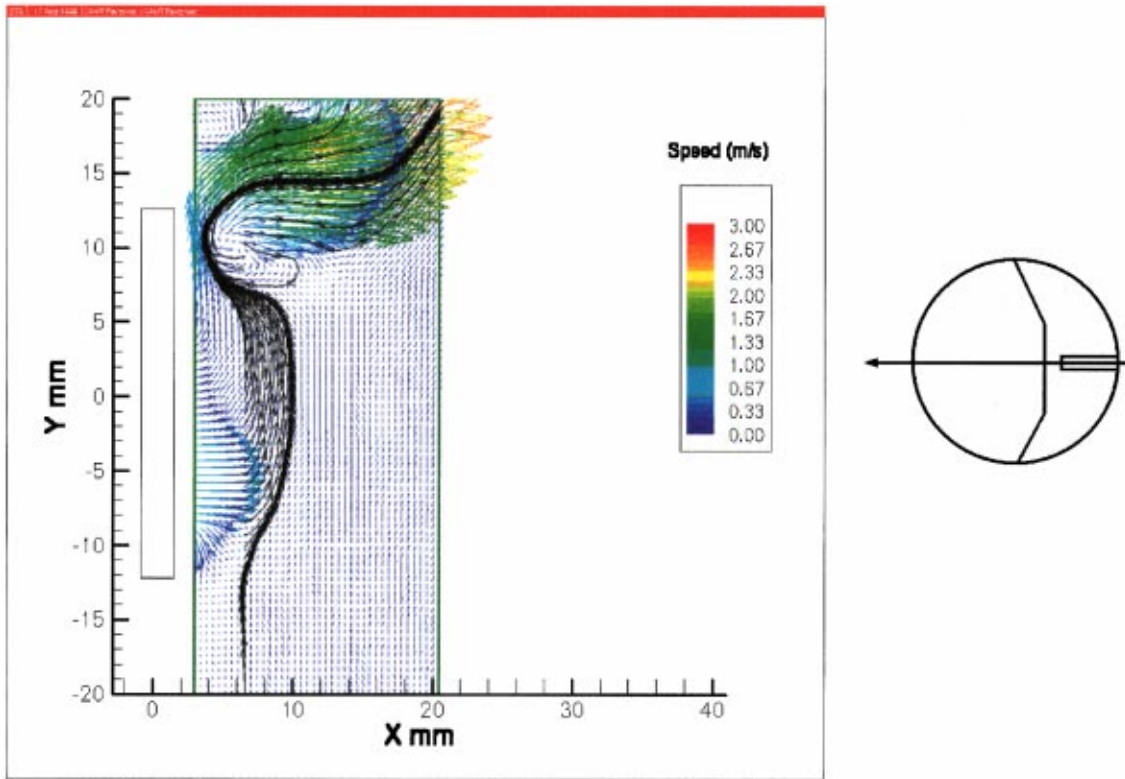
FIGURE 6. Streamlines as observed in the horizontal central plane ($z=0$ mm) during valve closure forward motion. Note that the map begins ~3 mm away from the actual valve seat. This map indicates the typical patterns marked A, B, and C.
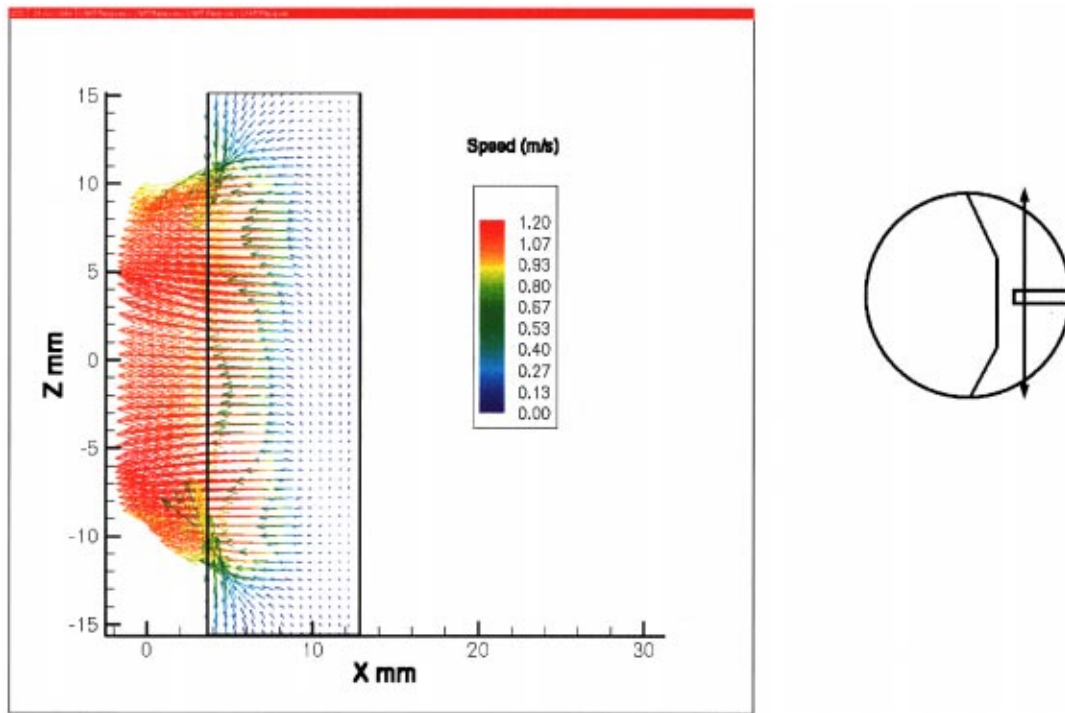

FIGURE 7. Average flow pattern in the vertical plane ($y=+6$ mm) on the minor orifice side during valve closure forward motion. Note that the map begins ~3 mm away from the actual valve seat. The flow indicated here is following the motion of the minor side of the occluder and indicates that there is a low pressure region created in the rear of the minor orifice side during the forward closure motion. This is the typical pattern marked C.
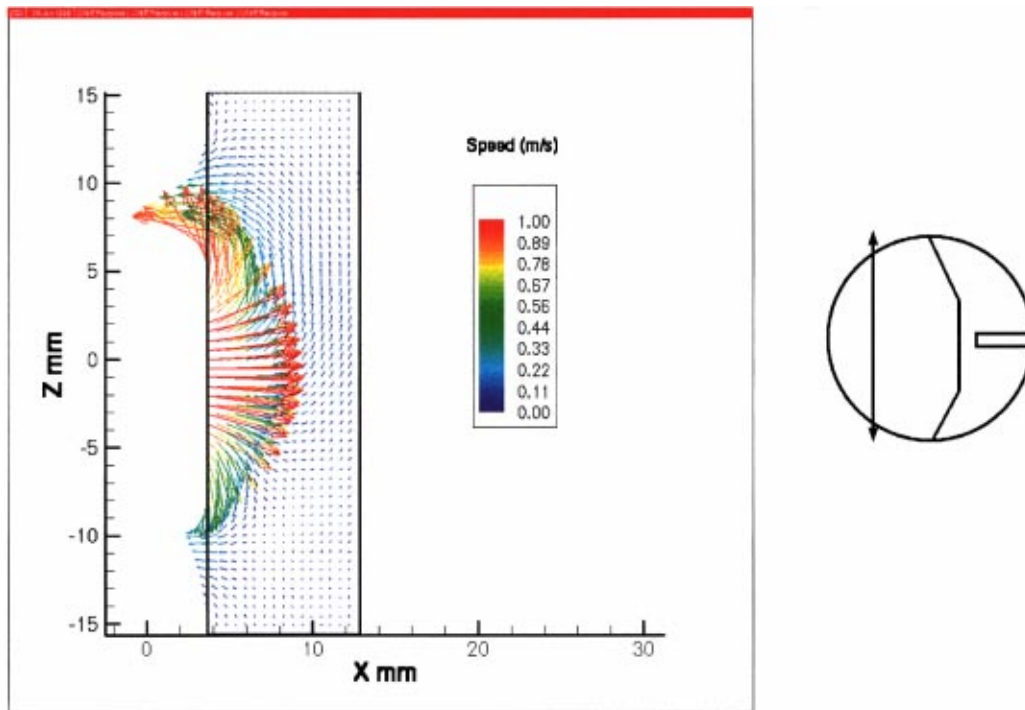
FIGURE 8. Average flow pattern in the vertical plane ($y = -6$ mm) on the major orifice side during valve closure forward motion. Note that the map begins ~3 mm away from the actual valve seat. The flow indicated here is following the motion of the major side of the occluder and a recirculation zone is observed as the jet enters the expansion zone in the atrial chamber. This is the typical pattern marked B.
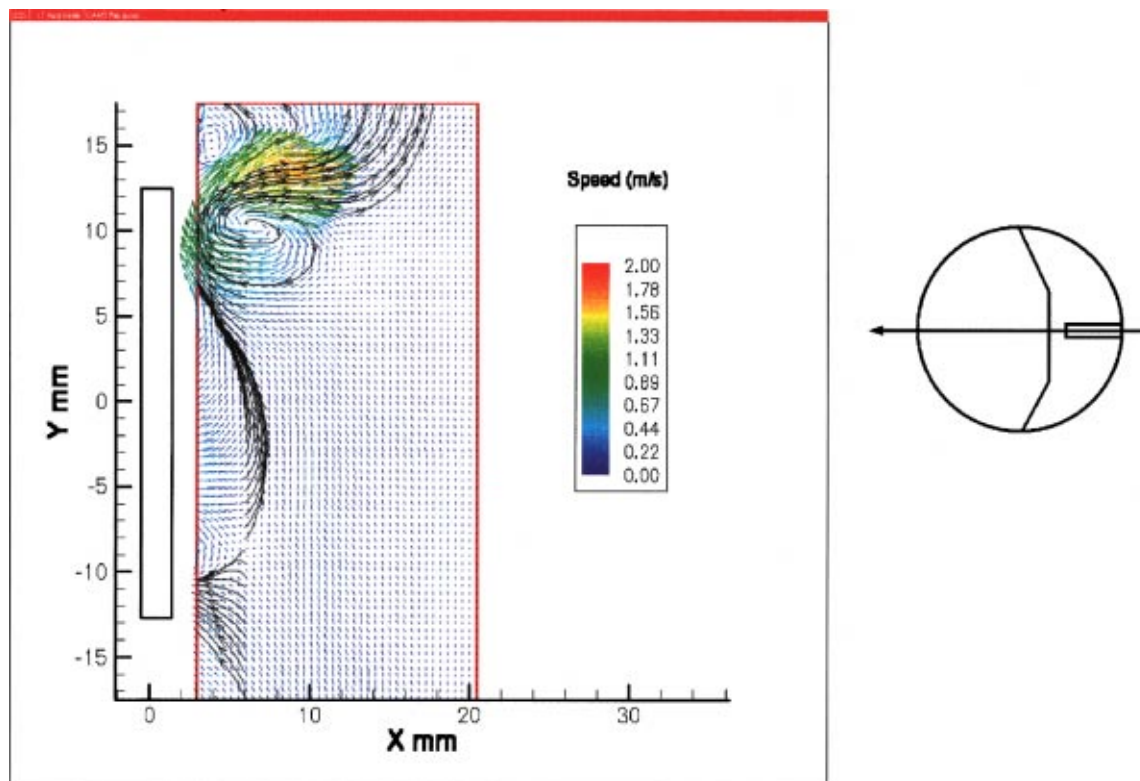

FIGURE 9. Streamlines in the horizontal central plane ($z = 0$ mm) during occluder rebound motion. Note that the map begins ~3 mm away from the actual valve seat. On the major orifice side, as seen here, the streamlines indicate the flow reversal leading to the rebound vortex.
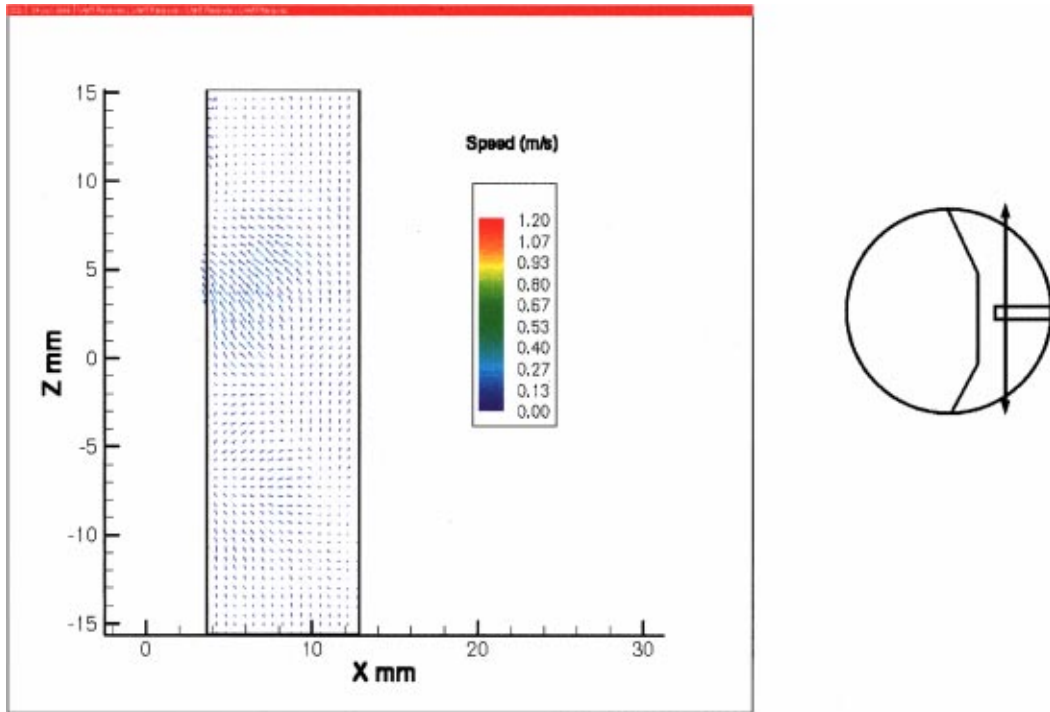
FIGURE 10. Average flow pattern in the vertical plane ($y=+6$ mm) on the minor orifice side during early valve rebound motion. Note that the map begins ~3 mm away from the actual valve seat. The flow pattern that followed the motion of the minor side of the occluder during closure forward motion is now absent.
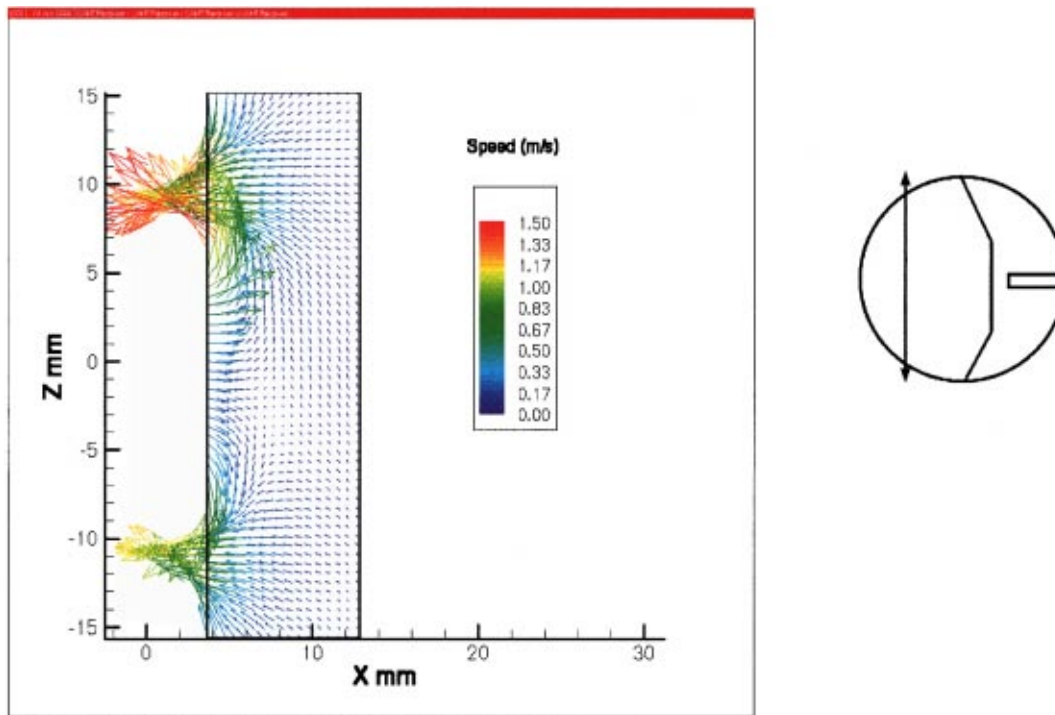

FIGURE 11. Average flow pattern in the vertical plane ($y=-6$ mm) on the major orifice side during valve closure rebound motion. Note that the map begins ~3 mm away from the actual valve seat. The flow indicated here along the periphery is drawn in by the local low (below atrial) pressure caused by the reverse rebound motion of the major side of the occluder. This is the typical pattern marked D and this is the region where cavitation fields are usually observed.

inertia of original flow profile associated with the fluid following the minor side (as was seen in Fig. 7) has been overcome. On the other hand, the experimentally determined flow patterns associated with region D, in the $y = -6$ mm vertical plane on the major orifice side during valve closure forward motion is depicted in Fig. 11. It can be seen that in this plane, measured at least 3 mm away from the valve seat, there is tendency to draw fluid in along the periphery due to the local sharp pressure drop created by the rebound. Note that the maps begin ~3 mm away from the actual valve seat and the inertia of the fluid has to be overcome in the central region where the fluid speed was high during the forward closure motion as was seen in Fig. 8.

CONCLUSIONS

Although the flow rate in real mitral valve operation is considerably higher in forward flow than in regurgitant flow, it has been held that the regurgitant flow plays a significant role in the hemolysis and blood element trauma associated with tilting heart disk valves because of various factors such as cavitation and elevated turbulent stresses.[6,8,17–19] The present study clearly depicts in spatial detail the flow patterns associated with the occluder motion, both in the forward closure phase, as well as the rebound phase. In particular, right after the instant of valve closure, a tension wave is created which causes a local pressure drop on the major orifice side. In addition, as the occluder is unable to dissipate its kinetic energy of closure, it rebounds, thus leading to a *further* pressure drop on the major orifice side. It is possible that the combination of the tension wave and the rebound effect may be sufficient to drive the local pressure below the vapor pressure and thereby generate vaporous cavitation. Thus, along the periphery of the major side of the occluder where the inertia of the fluid flow was small during forward closure, the fluid is rapidly drawn into this low pressure zone. This indicates that research and designs developed by Shu[12] in order to reduce the energy of closure by intentional dissipation may help in the reduction of the cavitation potential of such rigid valves.

Further it should be noted that this local pressure drop, flow reversal and the 3D vortex pattern are extremely short lived, because when the occluder rebounds the high pressure ventricular side gains access to the low pressure region and the pressure drop is quickly relieved. This short-lived nature of the pressure drop may explain why cavitation is initiated right after the instant of valve closure and is seldom seen beyond 2 ms after it, even though the rebound and return motion of the occluder is known to last ~10 ms. This is consistent with previous studies using the BSM valve which have indeed indicated that the most dominant cavitation fields are observed on the major orifice side and are extremely short

lived.[8,19] Also, these studies[8] indicate that the cavitation field is generated *within* 1 ms *after* the instant of valve closure and lasts for ~1–2 ms.

In conclusion, this study suggests that the sudden stopping and subsequent rebound motion of the occluder on the higher-speed major orifice side plays a role in the initiation of the vaporous cavitation field there. This would be consistent with the initiation of cavitation, because of the sharp local pressure drop created by the sudden stopping and rebound motion of the occluder on the major orifice side. While indicating that the sudden stop and subsequent rebound effect contributes to the cavitation phenomenon on the major orifice side of tilting-disk occluder MHVs by dropping the local, the present study in no way denies the involvement of other factors contributing to the formation of the cavitation field on the major orifice side of the BSM valve, such as scraping vortices and squeeze flows, even though no direct experimental evidence exists for these phenomena as yet. In particular, the theory of occluder rebound does not explain the mechanism for the cavitation frequently observed on the central orifice of the tilting-disk Medtronic Hall MHVs.

ACKNOWLEDGMENTS

REFERENCES

[1] Adrian, R. J., Particle Imaging Techniques for Experimental Fluid Mechanics. *Annu. Rev. Fluid Mech.* 23:261–304, 1991.

[2] Bluestein, D., S. Einav, and N. H. C. Hwang. A Squeeze Flow Phenomenon at the Closing of a Bileaflet Mechanical Heart Valve Prostheses. *J. Biomech.* 27:1369–1378, 1994.

[3] Chandran, K. B., C. S. Lee, and L. D. Chen. Pressure Field in the Vicinity of Mechanical Valve Occluders at the Instant of Valve Closure: Correlation with Cavitation Initiation. *J. Heart Valve Dis.* 3:565–576, 1994.

[4] Chandran, K. B., and S. Aluri. Mechanical Valve Closing Dynamics: Relationship between Velocity of Closing, Pressure Transients, and Cavitation Initiation. *Ann. Biomed. Eng.* 25:926–938, 1997.

[5] Farrell, K. J., and M. L. Billet. A Correlation of Leakage Vortex Cavitation in Axial-Flow Pumps. *J. Fluids Eng.* 116:551–557, 1994.

[6] Garrison, L. A., T. C. Lamson, S. Deutsch, D. B. Geselowitz, R. P. Gaumond, and J. M. Tarbell. An *In Vitro* Investigation of Prosthetic Heart Valve Cavitation in Blood. *J. Heart Valve Dis.* 3(1):7–24, 1994.

[7] Kafesian, R., M. Howanec, G. D. Ward, L. Diep, L. S. Wagstaff, and R. Rhee. Cavitation Damage of Pyrolytic Carbon in Mechanical Heart Valves. *J. Heart Valve Dis.* 3:52–57, 1994.

[8] Lamson, T. C., G. Rosenberg, S. Deutsch, D. B. Geselowitz, D. R. Stinebring, J. A. Frangos, and J. M. Tarbell. Relative Blood Damage in the Three Phases of a Prosthetic Heart Valve Flow Cycle. *ASAIO J.* 39:M626–M633, 1993.

[9] Lee, C. S., and K. B. Chandran. Instantaneous Back Flow Through Peripheral Clearance of Medtronic Hall Tilting Disc Valve at the Moment of Closure. *Ann. Biomed. Eng.* 22:371–380, 1994.

[10] Lee, C. S., and K. B. Chandran. Numerical Simulation of Instantaneous Back Flow Through Central Clearance of Bileaflet Mechanical Heart Valves at Closure: Shear Stress and Pressure Fields Within Clearance. *Med. Biol. Eng. Comput.* 33:257–263, 1995.

[11] Makhijani, V. B., H. Q. Yang, A. K. Singhal, and N. H. C. Hwang. An Experimental-Computational Analysis of MHV Cavitation: Effects of Leaflet Squeezing and Rebound. *J. Heart Valve Dis.* 3:535–548, 1994.

[12] Shu, M. Composite curvature bileaflet prosthetic heart valve with serpentine curve hinge recesses. US Patent No. 5,314,467 (24 May 1994).

[13] Wu, Z. J., and N. H. C. Hwang. Transient Pressure Signals as a Means in Measuring Mechanical Heart Valve Cavitation Potential. *Ann. Biomed. Eng.* 24(S1):S-2, 1996.

[14] Wu, Z. J., Y. Wang, and N. H. C. Hwang. Occluder Closing Behavior: A Key Factor in Mechanical Heart Valve Cavitation. *J. Heart Valve D. J.* 3:525–534, 1994.

[15] Young, F. R. Cavitation. London: McGraw-Hill, 1989.

[16] Zapanta, C. M., D. R. Stinebring, S. Deutsch, D. B. Geselowitz, and J. M. Tarbell. Continuing Investigations of In Vivo Prosthetic Heart Valve Cavitation. *Ann. Biomed. Eng.* 24(S1):S–4, 1996a.

[17] Zapanta, C. M., D. R. Stinebring, S. Deutsch, D. B. Geselowitz, and J. M. Tarbell. Correlation of Prosthetic Heart Valve Cavitation and Valve Leaflet Dynamics. *Ann. Biomed. Eng.* 24(S1):S–2, 1996b.

[18] Zapanta, C. M., D. R. Stinebring, S. Deutsch, D. B. Geselowitz, and J. M. Tarbell. In Vivo Observation of Cavitation on Prosthetic Heart Valves. *ASAIO Trans.* (in press).

[19] Zapanta, C. M., E. G. Liszka, T. C. Lamson, D. R. Stinebring, S. Deutsch, D. B. Geselowitz, and J. M. Tarbell. A Method for Real-Time *In Vitro* Observation of Cavitation on Prosthetic Heart Valves. *J. Biomed. Eng.* 116:460–468, 1994.